

Title	Studies on Divalent Ion Conducting Solid Electrolytes
Author(s)	李, 源洛
Citation	大阪大学, 2019, 博士論文
Version Type	VoR
URL	https://doi.org/10.18910/73550
rights	
Note	

Osaka University Knowledge Archive : OUKA

<https://ir.library.osaka-u.ac.jp/>

Osaka University

Doctoral Dissertation

Studies on Divalent Ion Conducting Solid Electrolytes

(2価イオンを伝導種とする新規なイオン伝導性固体に関する研究)

Wonrak Lee

July 2019

Department of Applied Chemistry

Graduate School of Engineering

Osaka University

Studies on Divalent Ion Conducting Solid Electrolytes

(2価イオンを伝導種とする新規なイオン伝導性固体に関する研究)

Wonrak Lee

2019

Department of Applied Chemistry

Graduate School of Engineering

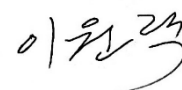
Osaka University

Preface

The work of this thesis has been carried out under the supervision of Professor Dr. Nobuhito Imanaka at Department of Applied Chemistry, Graduate School of Engineering, Osaka University.

The object of this thesis is to clarify the effects of crystal structure and constituent cations including conducting divalent cation on the divalent cation conducting properties in solids.

The author wishes that the findings and the knowledge obtained in this work will provide useful information for further development and design of novel solid electrolytes and that the materials would contribute to practical applications.



Wonrak Lee

Department of Applied Chemistry

Graduate School of Engineering

Osaka University

2-1 Yamadaoka, Suita,

Osaka 565-0871,

Japan

July 2019

Contents

<i>General Introduction</i>	1
<i>List of Publications</i>	4

Chapter 1

Novel Divalent Ni²⁺ Cation Conductor with NASICON-type Structure

1.1	Introduction	5
1.2	Experimental Procedure	5
1.3	Results and Discussion	7
1.4	Conclusions	15

Chapter 2

Novel Divalent Ca²⁺ Cation Conductor with NASICON-type Structure

2.1	Introduction	16
2.2	Experimental Procedure	17
2.3	Results and Discussion	18
2.4	Conclusions	23

Chapter 3

Effect of the Conducting Divalent Ion Species on the Ion Conducting in Solid Electrolytes with NASICON-type Structure

3.1	Introduction	24
3.2	Experimental Procedure	24
3.3	Results and Discussion	26
3.3.1	$(\text{Sr}_x\text{Hf}_{1-x})_{4/(4-2x)}\text{Nb}(\text{PO}_4)_3$ solid	26
3.3.2	$(\text{Ba}_x\text{Hf}_{1-x})_{4/(4-2x)}\text{Nb}(\text{PO}_4)_3$ solid	28
3.3.3	Comparison of $(\text{M}_x\text{Hf}_{1-x})_{4/(4-2x)}\text{Nb}(\text{PO}_4)_3$ solids	29
3.4	Conclusions	33
	<i>Summary</i>	34
	<i>References</i>	36
	<i>Acknowledgements</i>	39

General Introduction

Solid electrolyte is one of the promising candidates for the key component of next-generation electrochemical devices such as all-solid state batteries, chemical sensors, and fuel cells because of their high chemical and thermal stabilities in addition to high energy density [1-4]. Generally, in the solid electrolyte field, it is well accepted that ion migration in solid is strongly influenced by both ionic size and valence state of the conducting ion species. As the valence number of the conducting ion species increases, the electrostatic interaction with surrounding counter ions becomes stronger. Furthermore, the larger the ionic size of conducting ion species is, the harder the migration in the rigid crystal structure becomes because most of the solids have dense structure without enough open space for migration of bulky ions. As a result, the conduction of ions having large ionic size and/or high-valence number are considered to be poor migrant in crystalline solids [5]. Based on this theory, many researchers are focusing on ions with small size and low-valence state such as Li^+ and H^+ which are highly expected to migrate smoothly in solid lattice, and many kinds of Li^+ or H^+ ion conductors have been developed. However, due to the steady increase in demand of higher energy density for the next-generation batteries which can be applied to energy storage systems and electric vehicles, the divalent ion conductors that can theoretically carry twice electron compared to monovalent ion conductors if migration rate is the same are getting attention, and the small-size divalent Mg^{2+} ion is focused as a promising candidate for the conducting cation species in solids [6-9].

So far, several divalent cations such as Ni^{2+} , Mg^{2+} , Ca^{2+} , Sr^{2+} , Pb^{2+} , and Ba^{2+} have been reported to conduct in some solids with β'' -alumina or β - $\text{Fe}_2(\text{SO}_4)_3$ -type structures [10-14]. However, the ion conducting pathway in these crystal structures are layered or distorted three-dimensional network one which prohibits smooth ion migration in the crystal, and therefore, the divalent cation conductivities of these solids are so low that these solids cannot be applied for the practical use.

Although there are some reports on divalent cation (Ca^{2+} , Sr^{2+} , Pb^{2+} , and Ba^{2+}) conduction in well-ordered three-dimensional network structure of NASICON (Na^+ super ionic conductor)-type $\text{MZr}_4(\text{PO}_4)_6$ ($\text{M} = \text{Ca}^{2+}$, Sr^{2+} , Pb^{2+} , Ba^{2+}) solids [14-16], their conductivities were also significantly low even having the well-ordered network structure because of the strong electrostatic interaction between conducting cations and surrounding anions. These results imply that a new strategy is strongly required for developing the practically applicable divalent cation conductors; strict selection of both crystal structure and components is necessary for realizing smooth divalent cation conduction in solids.

It has been proposed the strategy for realization of high valent cation conduction in solids by the laboratory I belong; both the selection of the crystal structure holding well-ordered large conducting pathway for smooth ion migration and the effective reduction of strong electrostatic interaction. Based on this strategy, various kinds of trivalent and tetravalent cation conducting solids with well-ordered NASICON-type structure, have been reported [17-42]. Furthermore, this strategy is effective for the divalent cation conducting solids, and Imanaka research group reported the Mg^{2+} cation conducting $(\text{Mg}_{0.1}\text{Hf}_{0.9})_{4/3.8}\text{Nb}(\text{PO}_4)_3$ [9] solid with NASICON-type structure whose divalent Mg^{2+} conductivity was the highest among the Mg^{2+} cation conductors. The $(\text{Mg}_{0.1}\text{Hf}_{0.9})_{4/3.8}\text{Nb}(\text{PO}_4)_3$ solid contains Hf^{4+} , Nb^{5+} , and P^{5+} as the higher valent cations in its structure, which is the different point from the above mentioned NASICON-type $\text{MZr}_4(\text{PO}_4)_6$ ($\text{M} = \text{Ca}^{2+}$, Sr^{2+} , Pb^{2+} , Ba^{2+}) solids [14].

As mentioned above, the Mg^{2+} highly-conducting solid have been reported, but the key factors for providing the high divalent cation conductivity are not clarified, and further improvement of divalent cation conductivity or new divalent cation conductors with high conductivity can be expected when this point is made clear.

The aim of this thesis is to develop novel NASICON-type divalent cation conductor with high conductivity, with clarifying the key factors on divalent cation conduction in solids. For this

purpose, various kinds of NASICON-type divalent cation conductors and their conducting properties were discussed from the view point of constituent cations.

This thesis consists of the following three chapters.

In Chapter 1, the novel Ni^{2+} cation conductors, $(\text{Ni}_x\text{Hf}_{1-x})_{4/(4-2x)}\text{Nb}(\text{PO}_4)_3$ solids with NASICON-type structure, are described. By selecting Ni^{2+} cation having smaller ionic radius than Mg^{2+} cation, the divalent cation conductivity was successfully improved.

In Chapter 2, the divalent Ca^{2+} cation conduction in $(\text{Ca}_x\text{Hf}_{1-x})_{4/(4-2x)}\text{Nb}(\text{PO}_4)_3$ solids is studied. By introducing Ca^{2+} with electronegativity lower than Mg^{2+} into the Hf^{4+} ion site of the NASICON-type $\text{HfNb}(\text{PO}_4)_3$ solid, the electrostatic interaction was successfully weakened.

Chapter 3 discusses on the effect of the mobile divalent cation species on the ion conducting properties in the NASICON-type solids. For discussion, A ratio, ion conductivity, and activation energy of the divalent M^{2+} cation ($\text{M} = \text{Ni}, \text{Mg}, \text{Ca}, \text{Sr}$) conductors of the NASICON-type structure are described.

List of publications

1. Divalent Ni²⁺ Cation Conduction in NASICON-type Solid

Wonrak Lee, Shota Yamauchi, Shinji Tamura, Nobuhito Imanaka

Materials Letters, 2019, **234**, 261~263.

2. New Calcium Ion Conducting Solid Electrolyte with NASICON-type Structure

Wonrak Lee, Shinji Tamura, Nobuhito Imanaka

Chemistry Letters, 2017, **46**, 1486~1489.

3. Synthesis and Characterization of Divalent Ion Conductors with NASICON-type Structures

Wonrak Lee, Shinji Tamura, Nobuhito Imanaka

Journal of Asian Ceramic Societies, 2019, **7**, 221~227.

Chapter 1

Novel Divalent Ni²⁺ Cation Conductor with NASICON-type Structure

1.1 Introduction

Generally, the ionic radius of the conducting cations affect the ionic conductivity; conducting cation species with small ionic radius are easy to migrate in the structure. Actually, the (Mg_{0.1}Hf_{0.9})_{4/3.8}Nb(PO₄)₃ solid with NASICON-type structure exhibit has been reported to high Mg²⁺ cation conductivity [9]. Therefore, much higher conductivity can be expected by selecting smaller divalent cation than Mg²⁺ as the conducting species.

In order to develop novel divalent cation conductor with high ionic conductivity, Ni²⁺ (0.083 nm [coordination number = 6] [43]) ion having smaller ionic radius than that of Mg²⁺ (0.086 nm [coordination number = 6] [43]) ion was selected as conducting cation species. For comparing the divalent ion conductivity of the (Mg_{0.1}Hf_{0.9})_{4/3.8}Nb(PO₄)₃ solid, the NASICON-type HfNb(PO₄)₃ [42] was selected as the mother solid and the Ni²⁺ cation conducting properties in the (Ni_xHf_{1-x})_{4/(4-2x)}Nb(PO₄)₃ solids were investigated.

1.2 Experimental Procedure

(Ni_xHf_{1-x})_{4/(4-2x)}Nb(PO₄)₃ solids were synthesized by a conventional co-precipitation method using Ni(NO₃)₂, HfCl₄, NbCl₅, and (NH₄)₂HPO₄ as starting materials. (NH₄)₂HPO₄ diluted in 3 N HNO₃ was added into an ethanol solution dissolved Ni(NO₃)₂, HfCl₄, and NbCl₅. The mixed solution

was stirred at 130 °C for 24 h to obtain a precipitate, which was collected and dried at 130 °C for several hours. The obtained powders were calcined at 600 °C for 6 h, and then the sample powders were pelletized and calcined again at 1100 °C for 6 h, 1200 °C for 6 h, and 1300 °C for 6 h under an air atmosphere. The synthesized samples were characterized using X-ray powder diffraction (XRD) with Cu K α radiation (SmartLab, Rigaku), with a step scanning method in the 2θ range between 10 and 40° and a step width of 0.04°. Lattice volumes of the samples were calculated based on the XRD peak angles with α -Al₂O₃ powder as an internal standard reference. After identifying the crystal phase of the (Ni_xHf_{1-x})_{4/(4-2x)}Nb(PO₄)₃ powders, the sample powders were pelletized and sintered at 1300 °C for 12 h under an air atmosphere. X-ray photoelectron spectroscopy (XPS; PHI5000 VersaProbe II. ULVAC-PHI) was performed using Al K α radiation.

Electrical conductivity of the sintered sample pellets was measured with sputtered platinum layers formed on the center of each side of the pellet, and the ac conductivity (σ_{ac}) of the sintered sample pellets was measured by means of the complex impedance method in the frequency range between 5 and 13M Hz (1260 Impedance/Gain-Phase Analyzer, Solartron) at temperatures ranging from 300 to 600 °C, under an air atmosphere. Both ac and dc conductivities were measured at 600 °C in various oxygen partial pressures ranging from 10⁻¹⁶ to 10⁵ Pa, which were obtained by regulating an O₂, Ar, and CO-CO₂ gas mixture, to identify the conducting species in the (Ni_{0.06}Hf_{0.94})_{4/3.88}Nb(PO₄)₃ solid. Dc electrolysis of the (Ni_{0.06}Hf_{0.94})_{4/3.88}Nb(PO₄)₃ pellet sandwiched by platinum bulk electrodes was carried out by applying a dc voltage of 4 V for 25 days at 650 °C under an air atmosphere. After the dc electrolysis, cross-sectional line analysis using energy dispersive X-ray spectroscopy (EDX; SSX-550, Shimadzu) was carried out to investigate the elemental distribution inside the electrolyzed sample pellet.

1.3 Results and Discussion

Figure 1.1 shows the XRD patterns for the $(\text{Ni}_x\text{Hf}_{1-x})_{4/(4-2x)}\text{Nb}(\text{PO}_4)_3$ ($0.03 \leq x \leq 0.10$) solids after calcination at 1300 °C. For all samples, diffraction pattern corresponded to the trigonal NASICON-type structure with space group $R\bar{3}c$ was observed, and only the samples with $x \leq 0.06$ were obtained as a single-phase NASICON-type solid. For the samples with $x > 0.06$, impurity phases of HfP_2O_7 and NbPO_5 were also formed in addition to the NASICON-type phase. Furthermore, the peaks assigned to the NASICON-type phase shifted to higher angles with an increase in Ni content (x) up to 0.06, although it is difficult to recognize this peak shift from the figure because of a small difference in ionic radius between Ni^{2+} (0.083 nm [CN = 6] [43]) and Hf^{4+} (0.085 nm [CN = 6] [43]), and due to the relatively low amount of doped Ni^{2+} .

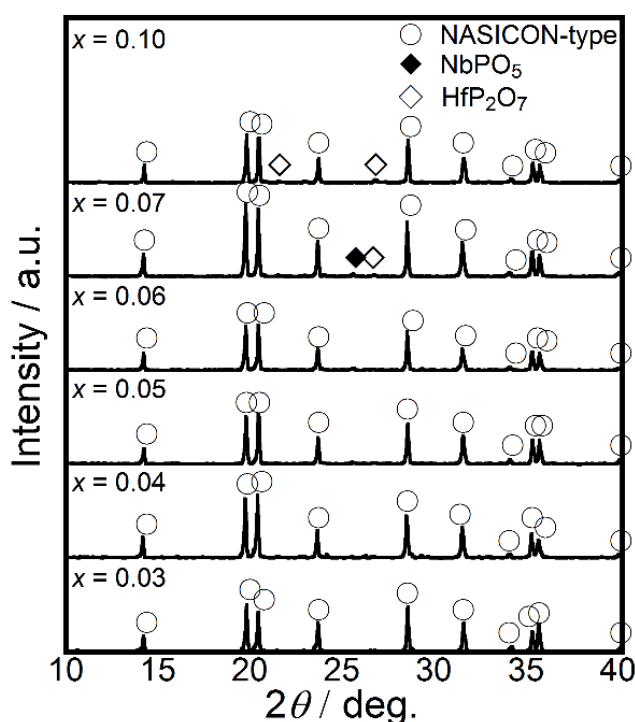


Figure 1.1. X-ray diffraction (XRD) patterns of the $(\text{Ni}_x\text{Hf}_{1-x})_{4/(4-2x)}\text{Nb}(\text{PO}_4)_3$ ($0.03 \leq x \leq 0.10$) solids after the calcination at 1300°C.

Figure 1.2 displays the compositional dependence of lattice volume of the NASICON-type phase for the prepared samples. The lattice volumes of the single-phase samples ($x \leq 0.06$) with NASICON-type structure were linearly decreased with increasing Ni content (x) because of smaller size of Ni^{2+} cation (0.083 nm [CN = 6] [43]) than that of Hf^{4+} cation (0.085 nm [CN = 6] [43]). In contrast, any significant lattice volume changes were not observed for the multi-phase samples with $x > 0.06$. From this result, it is clear that the small-size Ni^{2+} ions were successfully substituted the Hf^{4+} cation sites, and that the compositional solid solubility limit was $x = 0.06$.

Figure 1.2 also shows the compositional dependencies of the ac conductivity at 600 °C and the activation energy for Ni^{2+} ion conduction (Ni^{2+} migration is demonstrated afterward.) which was estimated from the ac conductivities at temperatures from 300 to 600 °C. Parallel to the lattice volume change, the conductivity increased and the activation energy decreased with an increase in Ni content (x) up to 0.06. The highest conductivity ($2.27 \times 10^{-4} \text{ S} \cdot \text{cm}^{-1}$ at 600 °C) and the lowest activation energy ($50.0 \text{ kJ} \cdot \text{mol}^{-1}$) were obtained for the $(\text{Ni}_{0.06}\text{Hf}_{0.94})_{4/3.88}\text{Nb}(\text{PO}_4)_3$ solid with the solid solubility limit composition. On the other hand, in multi-phase samples with $x > 0.06$, conductivity decreased and activation energy increased, due to the formation of impurity phases such as HfP_2O_7 and NbPO_5 which prohibit the Ni^{2+} conduction between sample grains.

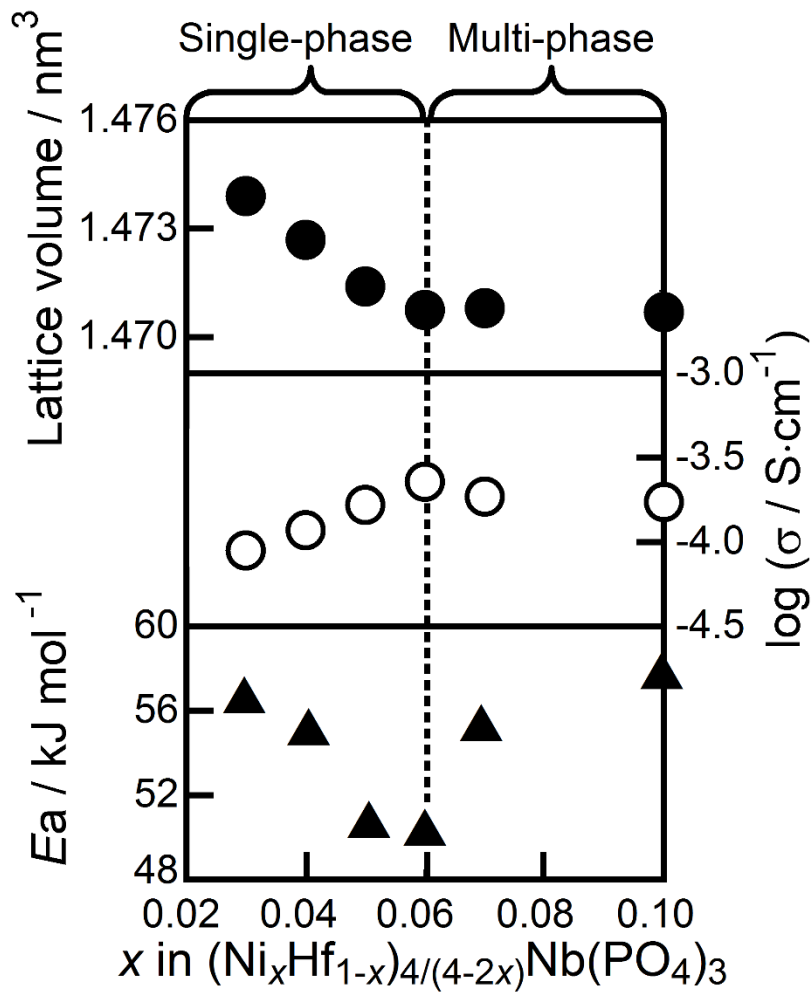


Figure 1.2. Compositional dependencies of the lattice volume (●), ac conductivity at 600 °C (○), and the activation energy (▲) for the $(\text{Ni}_x\text{Hf}_{1-x})_{4/(4-2x)}\text{Nb}(\text{PO}_4)_3$ solids.

Figure 1.3 depicts the EDX cross-sectional line analysis result for the electrolyzed $(\text{Ni}_{0.06}\text{Hf}_{0.94})_{4/3.88}\text{Nb}(\text{PO}_4)_3$ solid after applying a dc voltage of 4 V for 25 days at 650 °C in air atmosphere. Deposition of Ni was clearly evident at the cathodic surface of the sample pellet, while no peaks corresponding to other cation species such as Hf^{4+} , Nb^{5+} , or P^{5+} were observed, which suggests that only Ni^{2+} migrated from the anodic side to the cathodic surface via the potential gradient.

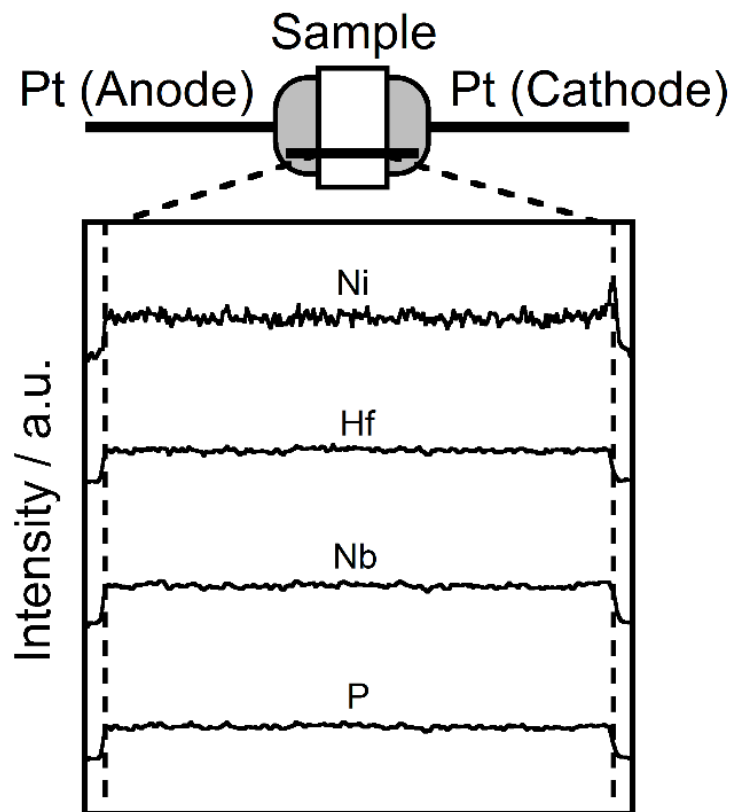


Figure 1.3. Results of EDX line analysis of the dc electrolyzed $(\text{Ni}_{0.06}\text{Hf}_{0.94})_{4/3.88}\text{Nb}(\text{PO}_4)_3$ solid.

The XPS spectrum of the area of the Ni 2p core levels for the $(\text{Ni}_{0.06}\text{Hf}_{0.94})_{4/3.88}\text{Nb}(\text{PO}_4)_3$ solid is shown in Figure 1.4. Only the peaks for two Ni 2p core levels, Ni 2p_{1/2} and Ni 2p_{3/2}, were observed, at 873.6 eV and 855.5 eV, respectively. These peaks were thus assigned to the divalent Ni²⁺ species. The spectrum of the Ni 2p state also contains two satellite peaks, at 879.5 eV and 861.2 eV [44-46].

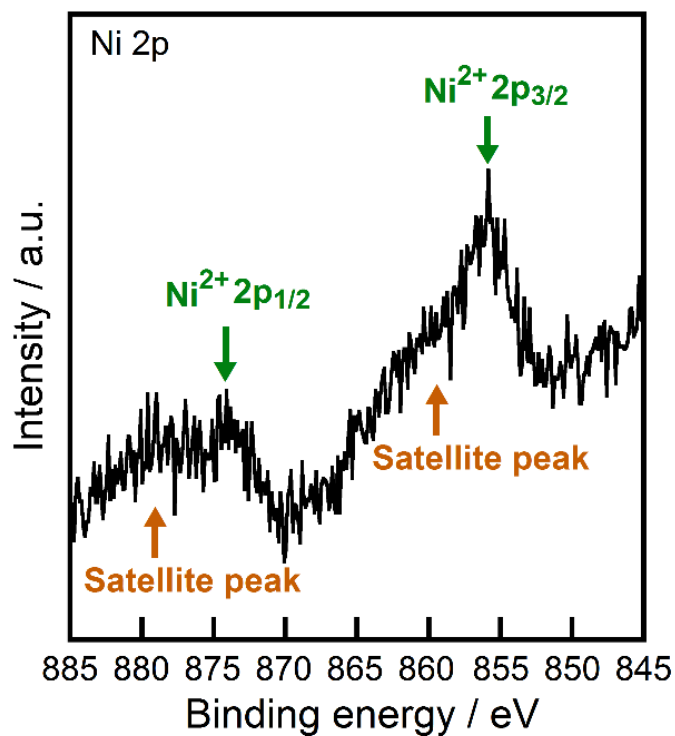


Figure 1.4. Ni 2p XPS spectrum of the $(\text{Ni}_{0.06}\text{Hf}_{0.94})_{4/3.88}\text{Nb}(\text{PO}_4)_3$ solid.

Figure 1.5 shows the dc conductivity ratio to ac one (σ_{dc}/σ_{ac}) for the $(\text{Ni}_{0.06}\text{Hf}_{0.94})_{4/3.88}\text{Nb}(\text{PO}_4)_3$ solid at 600 °C under O_2 or Ar atmosphere. The dc conductivity was measured by applying a 0.02 V dc voltage which is lower than the decomposition voltage (0.84 V). The dc conductivity obtained by applying a low dc voltage provides information about the contribution of conducting species. For example, in the case of the oxide anion (O^{2-}) being the conducting species, the dc conductivity is almost the same as the ac conductivity under the O_2 atmosphere because the conducting species is continuously supplied from the atmospheric O_2 . As a result, the σ_{dc}/σ_{ac} value remains stable even as time passes. However, under a reducing atmosphere (Ar), the dc conductivity decreases drastically with time because such atmosphere cannot supply the conducting species (O^{2-}). For electronic conductors, dc conductivity should be the same as ac conductivity under any atmosphere because conducting electrons can be supplied from the electrode, meaning that the σ_{dc}/σ_{ac} value would be unity under any atmosphere. On the other hand, for cation-conducting solids, the conducting species cannot be supplied from the atmosphere, nor the electrode if irreversible electrodes such as Pt are used. Therefore, the σ_{dc}/σ_{ac} ratio reduces drastically over time.

The σ_{dc}/σ_{ac} ratio for the $(\text{Ni}_{0.06}\text{Hf}_{0.94})_{4/3.88}\text{Nb}(\text{PO}_4)_3$ solid was reduced just after the dc conductivity measurement and the value decreased below 0.01 after 30 min under both O_2 and Ar atmospheres. This phenomenon strongly suggests that the conducting species in the $(\text{Ni}_{0.06}\text{Hf}_{0.94})_{4/3.88}\text{Nb}(\text{PO}_4)_3$ solid is neither O^{2-} ion nor electrons, but cations. Moreover, the cationic transference number (t_{cation}) of the $(\text{Ni}_{0.06}\text{Hf}_{0.94})_{4/3.88}\text{Nb}(\text{PO}_4)_3$ sample can be estimated to be 0.99 from the equation, $t_{\text{cation}} = 1 - (\sigma_{dc}/\sigma_{ac})$, because the σ_{dc}/σ_{ac} value for the cation conductor indicates the contribution of species other than cations to the conductivity [47].

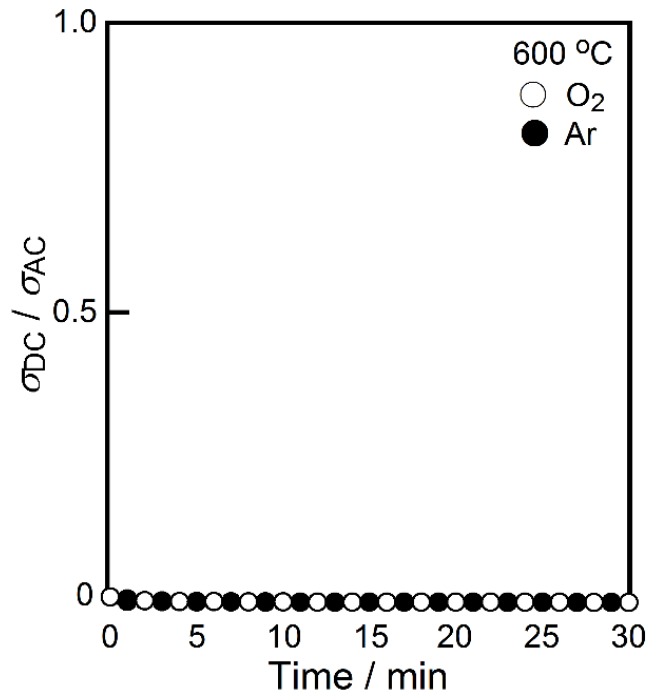


Figure 1.5. Time dependencies of the (σ_{dc}/σ_{ac}) ratio for the $(\text{Ni}_{0.06}\text{Hf}_{0.94})_{4/3.88}\text{Nb}(\text{PO}_4)_3$ solid in O_2 or Ar atmosphere.

Figure 1.6 shows the temperature dependence of the divalent cation conductivity for the NASICON-type $(\text{Ni}_{0.06}\text{Hf}_{0.94})_{4/3.88}\text{Nb}(\text{PO}_4)_3$ and $(\text{Mg}_{0.1}\text{Hf}_{0.9})_{4/3.8}\text{Nb}(\text{PO}_4)_3$ [9] solids with the corresponding data for the $\text{MZr}_4(\text{PO}_4)_6$ ($\text{M} = \text{Ni}, \text{Ca}, \text{Sr}, \text{Ba}$) [14] solids. The $(\text{Ni}_{0.06}\text{Hf}_{0.94})_{4/3.88}\text{Nb}(\text{PO}_4)_3$ (50 kJ mol^{-1}) solid exhibited higher cation conductivity and lower activation energy compared to $(\text{Mg}_{0.1}\text{Hf}_{0.9})_{4/3.8}\text{Nb}(\text{PO}_4)_3$ (53.8 kJ mol^{-1}) solid, because of the small ionic radius of Ni^{2+} cation (0.083 nm [CN = 6] [43]) than that of Mg^{2+} cation (0.086 nm [CN = 6] [43]), allowing smooth cation migration in the crystal structure. Furthermore, the $(\text{Ni}_{0.06}\text{Hf}_{0.94})_{4/3.88}\text{Nb}(\text{PO}_4)_3$ solid exhibited higher Ni^{2+} ion conductivity than $\beta\text{-Fe}_2(\text{SO}_4)_3$ -type $\text{NiZr}_4(\text{PO}_4)_6$ solid, and the ion conductivity at $600 \text{ }^\circ\text{C}$ was about 23 times higher than that of the

$\text{NiZr}_4(\text{PO}_4)_6$ solid. Moreover, the activation energy of Ni^{2+} cation conduction for the $(\text{Ni}_{0.06}\text{Hf}_{0.94})_{4/3.88}\text{Nb}(\text{PO}_4)_3$ solid was lower than that of the $\text{NiZr}_4(\text{PO}_4)_6$ (123 kJ mol^{-1}) solid. This is because the NASICON-type $(\text{Ni}_{0.06}\text{Hf}_{0.94})_{4/3.88}\text{Nb}(\text{PO}_4)_3$ solid has the well-ordered three-dimensional ion conducting pathway, while the $\text{NiZr}_4(\text{PO}_4)_6$ solid holds the distorted $\beta\text{-Fe}_2(\text{SO}_4)_3$ -type structure. In addition, the existence of high-valence cation such as Nb^{5+} in the structure effectively reduced the electrostatic interaction between migrating Ni^{2+} ions and the surrounding O^{2-} anions.

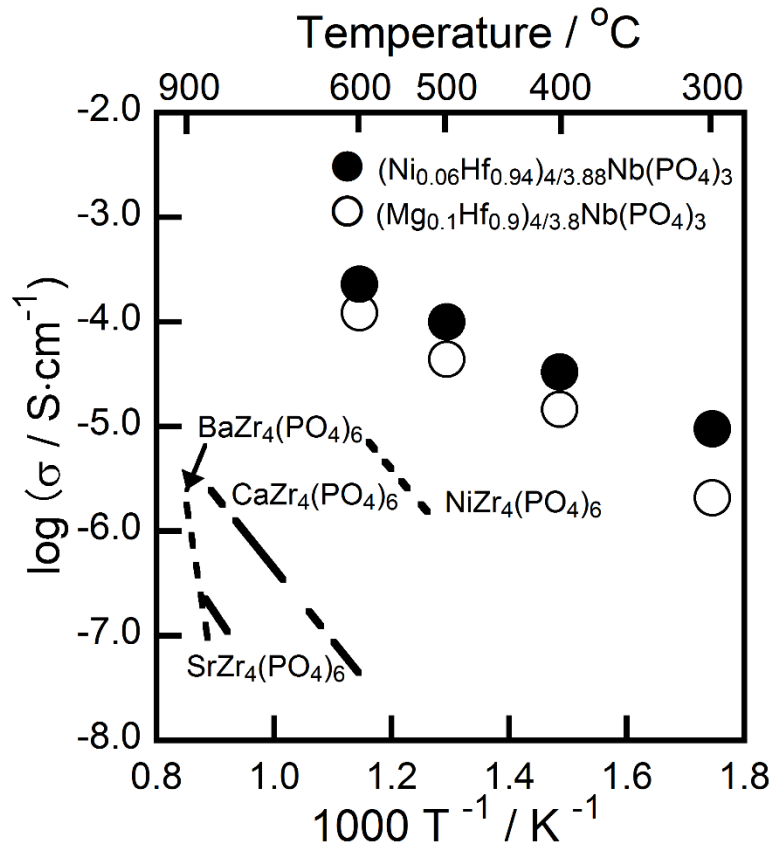


Figure 1.6. Temperature dependencies of the ac conductivity for the $(\text{Ni}_{0.06}\text{Hf}_{0.94})_{4/3.88}\text{Nb}(\text{PO}_4)_3$ (●), $(\text{Mg}_{0.1}\text{Hf}_{0.9})_{4/3.8}\text{Nb}(\text{PO}_4)_3$ (○), and $\text{MZr}_4(\text{PO}_4)_6$ (M = Ca (- -), Sr (—), Ba (--), Ni (···)) solids.

1.4 Conclusions

In order to develop a divalent cation conductor exhibiting high ion conductivity, $(\text{Ni}_x\text{Hf}_{1-x})_{4/(4-2x)}\text{Nb}(\text{PO}_4)_3$ were synthesized by partially substituting the Hf^{4+} ion site of the mother solid $\text{HfNb}(\text{PO}_4)_3$ with the Ni^{2+} ion whose ionic radius is smaller than Mg^{2+} . The $(\text{Ni}_{0.06}\text{Hf}_{0.94})_{4/3.88}\text{Nb}(\text{PO}_4)_3$ solid having the solid solubility limit composition exhibited the highest ionic conductivity ($2.27 \times 10^{-4} \text{ S} \cdot \text{cm}^{-1}$ at $600 \text{ }^\circ\text{C}$) and the lowest activation energy ($50 \text{ kJ} \cdot \text{mol}^{-1}$) which is higher conductivity and lower activation energy than those of previously reported $(\text{Mg}_{0.1}\text{Hf}_{0.9})_{4/3.8}\text{Nb}(\text{PO}_4)_3$, due to the smaller ionic radius of conducting species.

Chapter 2

Novel Divalent Ca²⁺ Cation Conductor with NASICON-type Structure

2.1 Introduction

The divalent Ni²⁺ cation conduction in the NASICON-type (Ni_{0.06}Hf_{0.94})_{4/3.88}Nb(PO₄)₃ solid was described in Chapter 1, and it was demonstrated that the effectiveness of selection for small cation as the conducting species in order to obtain high divalent cation conductivity. On the other hand, the ion migration in rigid crystal should also be influenced by the interaction between conducting ions and surrounding counter ions. As described in Chapter 1 of this thesis, I proposed that the introduction of higher valence cations than the conducting divalent cation was essential to improve the divalent cation conduction in solids. However, there is a possibility to reduce the electrostatic interaction between conducting divalent cations and surrounding oxide anions by the selection of divalent cations with lower electronegativity.

Among the divalent cations, calcium ion (Ca²⁺) has relatively low electronegativity of 1.0, implying that high Ca²⁺ ion conduction can be expected by selecting NASICON-type structure containing high valence cations such as Hf⁴⁺, Nb⁵⁺, and P⁵⁺, while its ionic radius is large and might be not suitable for migration in rigid lattice. Therefore in this chapter, a new Ca²⁺ conducting (Ca_xHf_{1-x})_{4/(4-2x)}Nb(PO₄)₃ solids were developed and their Ca²⁺ conducting properties were investigated.

2.2 Experimental Procedure

The $(\text{Ca}_x\text{Hf}_{1-x})_{4/(4-2x)}\text{Nb}(\text{PO}_4)_3$ solids were synthesized by the conventional wet coprecipitation method with $\text{Ca}(\text{NO}_3)_2$, HfCl_4 , NbCl_5 , and $(\text{NH}_4)_2\text{HPO}_4$ as starting materials. Stoichiometric amount of $(\text{NH}_4)_2\text{HPO}_4$ diluted in 3 N nitric acid solution was added dropwise into the mixed ethanol solution dissolved $\text{Ca}(\text{NO}_3)_2$, HfCl_4 , and NbCl_5 . The mixed solution was stirred and dried at 130 °C. The obtained powders were pre-calcined at 600 °C for 6 h, then pelletized and calcined at 1100 °C for 6 h. The obtained powders were repeatedly calcined at 1200 °C for 6 h until the solid state reaction was completed in air atmosphere.

X-ray powder diffraction (XRD; SmartLab, Rigaku) was measured with $\text{Cu K}\alpha$ radiation (40 kV, 40 mA) in 2θ range between 10 and 40°. The lattice volume of the calcined powders was calculated based on XRD peak angles, which was refined by using $\alpha\text{-Al}_2\text{O}_3$ powder as an internal standard reference. After identification of the crystal phase of the samples, $(\text{Ca}_x\text{Hf}_{1-x})_{4/(4-2x)}\text{Nb}(\text{PO}_4)_3$ powders were pelletized and sintered at 1200 °C for 12 h in air atmosphere.

The ac conductivity of the sample pellets sputtered with a Pt-layer on the center of both surfaces was measured by using a complex impedance method (1260 Impedance/Gain-Phase Analyzer, Solartron) in the frequency (5 Hz–13 MHz) at temperatures from 300 to 600 °C under air atmosphere. In order to identify the conducting species, both ac and dc conductivities were measured at 600 °C in various oxygen partial pressures from 10^{-17} to 10^5 Pa for the $(\text{Ca}_{0.05}\text{Hf}_{0.95})_{4/3.9}\text{Nb}(\text{PO}_4)_3$ solid.

The dc electrolysis was carried out for the sintered $(\text{Ca}_{0.05}\text{Hf}_{0.95})_{4/3.9}\text{Nb}(\text{PO}_4)_3$ solid by applying a dc voltage higher than the samples decomposition voltage in air atmosphere, and the elemental distribution in the electrolyzed pellets was examined by cross-sectional line analysis using energy dispersive X-ray spectroscopy (EDX; SSX-550, Shimadzu).

2.3 Results and Discussion

Figure 2.1 shows the results of XRD patterns for the $(\text{Ca}_x\text{Hf}_{1-x})_{4/(4-2x)}\text{Nb}(\text{PO}_4)_3$ ($0.01 \leq x \leq 0.10$) solids. The XRD patterns of $(\text{Ca}_x\text{Hf}_{1-x})_{4/(4-2x)}\text{Nb}(\text{PO}_4)_3$ solids with $x \leq 0.05$ showed single phase NASICON-type structure with space group $R\bar{3}c$, while solids with $x > 0.05$ observed additional impurity phase of NbPO_5 together with the NASICON-type phase. From the XRD peak angles, the lattice volume of the NASICON-type phase was calculated and the compositional dependence of the lattice volume is presented in Figure 2.2. The lattice volume of the NASICON-type phase for the single-phase samples ($x \leq 0.05$) increased with increasing Ca content (x) because of large ionic radius of Ca^{2+} cation (0.114 nm [CN = 6] [43]) than that of Hf^{4+} cation (0.085 nm [CN = 6] [43]). On the other hand, further increase of lattice volume was not observed in the compositional range where the impurity phase appeared. This result strongly indicates that the Ca^{2+} cations partially substitute the Hf^{4+} sites into the $\text{HfNb}(\text{PO}_4)_3$ solid for the samples with $x \leq 0.05$.

Figure 2.2 also depicts the compositional dependence of the ac conductivity for the samples with $x \leq 0.10$. Parallel to the lattice volume change, the conductivity monotonically increased with the Ca^{2+} content (x) up to $x = 0.05$, due to the increase of conducting Ca^{2+} amount in the solid. However, in the multi-phase region, the conductivity decreased, which was caused by the formation of insulating materials of NbPO_5 . This result also indicates that the solid solubility composition of the $(\text{Ca}_x\text{Hf}_{1-x})_{4/(4-2x)}\text{Nb}(\text{PO}_4)_3$ solids of NASICON-type structure was $x = 0.05$.

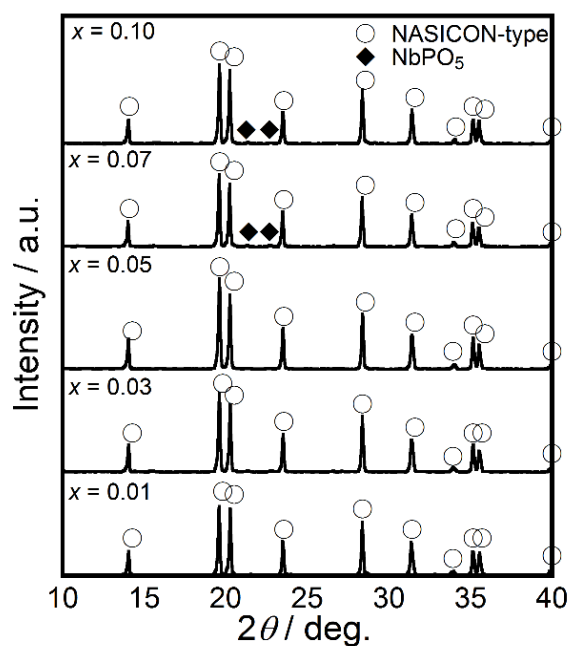


Figure 2.1. XRD patterns of the $(\text{Ca}_x\text{Hf}_{1-x})_{4/(4-2x)}\text{Nb}(\text{PO}_4)_3$ solids calcined at 1200 °C.

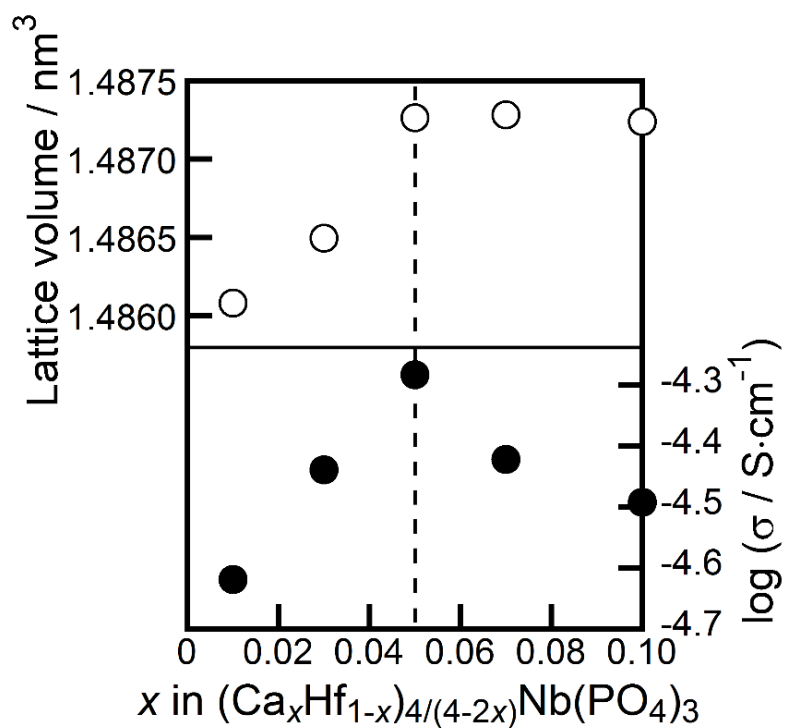


Figure 2.2. Compositional dependencies of the lattice volume (○) and the ac conductivity (●) of the $(\text{Ca}_x\text{Hf}_{1-x})_{4/(4-2x)}\text{Nb}(\text{PO}_4)_3$ solids.

Figure 2.3 depicts the oxygen partial pressure dependence of the ac conductivity at 600 °C for the $(\text{Ca}_{0.05}\text{Hf}_{0.95})_{4/3.9}\text{Nb}(\text{PO}_4)_3$ solid. In the case of metal oxides, oxygen species in the solid is generally released in the atmosphere with low oxygen partial pressure, generating the n-type electron conducting nature in the metal oxides. On the other hand, at high oxygen partial pressure, p-type hole conducting nature appears due to the oxidation of metal cation. Moreover, in the oxygen partial pressure region where ion conduction is dominant in solids, it is known that conductivity maintains without influence of oxygen partial pressure change. The $(\text{Ca}_{0.05}\text{Hf}_{0.95})_{4/3.9}\text{Nb}(\text{PO}_4)_3$ solid exhibited a constant electrical conductivity at the oxygen partial pressure range between 10^{-8} and 10^5 Pa, meaning that there is no possibility of electronic species (electron and hole) conduction in the sample in such wide oxygen partial pressure range. The $\sigma_{\text{dc}} / \sigma_{\text{ac}}$ conductivity ratio rapidly decreased with time and the value reached below 0.01 after 30 minutes under both Ar and O₂ atmospheres, which suggests that the cation transference number was over 0.99. From these results, the conducting species in the $(\text{Ca}_{0.05}\text{Hf}_{0.95})_{4/3.9}\text{Nb}(\text{PO}_4)_3$ solid are found to be the constituent cations (Ca^{2+} , Hf^{4+} , Nb^{5+} , and P^{5+}).

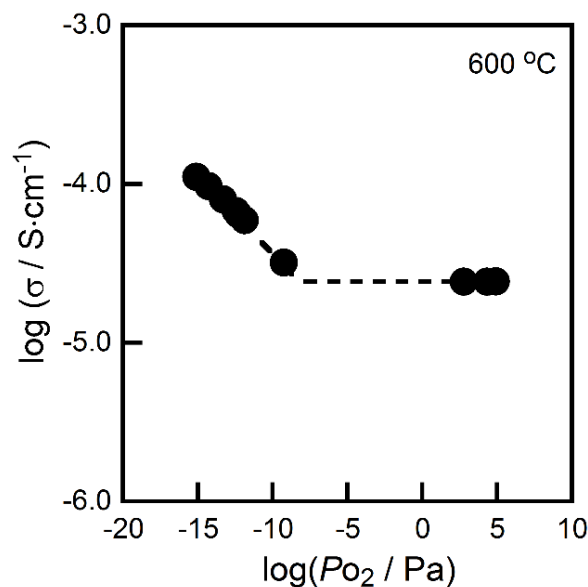


Figure 2.3. Relationship between the ac conductivity and the oxygen partial pressure for the $(\text{Ca}_{0.05}\text{Hf}_{0.95})_{4/3.9}\text{Nb}(\text{PO}_4)_3$ solid at 600 °C.

For the direct identification of Ca^{2+} cation migration in the $(\text{Ca}_{0.05}\text{Hf}_{0.95})_{4/3.9}\text{Nb}(\text{PO}_4)_3$ solid, dc electrolysis was carried out by applying 4 V dc voltage, which is higher than the decomposition voltage (ca. 1.1 V), to the sintered pellet at 650 °C for 14 days. By applying a dc voltage for the sample, only the conducting cations species should migrate to cathodic direction according to the potential gradient. Figure 2.4 depicts the EDX cross-sectional line analysis result of the $(\text{Ca}_{0.05}\text{Hf}_{0.95})_{4/3.9}\text{Nb}(\text{PO}_4)_3$ solid after the dc electrolysis. Deposition of Ca was clearly segregated at the cathodic surface of the sample pellet, while such deposition was not observed at the cathodic surface or inside of the sample pellet for other cation species such as Hf^{4+} , Nb^{5+} , or P^{5+} . This result clearly demonstrates the fact that only divalent Ca^{2+} ions conduct in the solid.

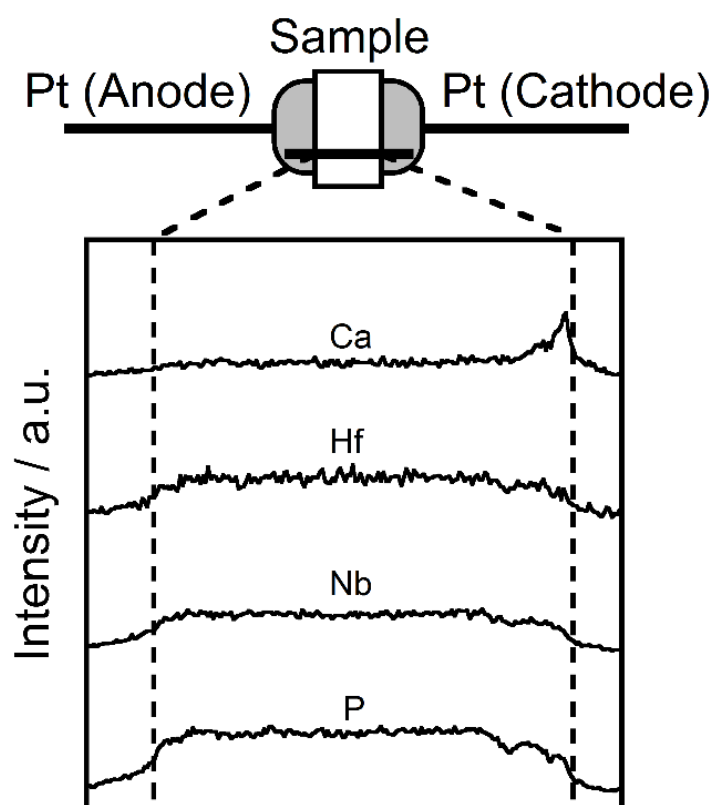


Figure 2.4. Results of EDX line analysis of the dc electrolyzed $(\text{Ca}_{0.05}\text{Hf}_{0.95})_{4/3.9}\text{Nb}(\text{PO}_4)_3$ solid.

Figure 2.5 shows the temperature dependencies of the divalent cation conductivity for the $(\text{Ca}_{0.05}\text{Hf}_{0.95})_{4/3.9}\text{Nb}(\text{PO}_4)_3$ and $(\text{Mg}_{0.05}\text{Hf}_{0.95})_{4/3.9}\text{Nb}(\text{PO}_4)_3$ solids with corresponding data for the NASICON-type $\text{CaZr}_4(\text{PO}_4)_6$ solid. The conductivity of the $(\text{Ca}_{0.05}\text{Hf}_{0.95})_{4/3.9}\text{Nb}(\text{PO}_4)_3$ solid was ca. 1000 times higher than that of the $\text{CaZr}_4(\text{PO}_4)_6$ solid at 600 °C. Moreover, the activation energy for Ca^{2+} ion conduction in the $(\text{Ca}_{0.05}\text{Hf}_{0.95})_{4/3.9}\text{Nb}(\text{PO}_4)_3$ solid ($55.80 \text{ kJ}\cdot\text{mol}^{-1}$) is lower than that of the $\text{CaZr}_4(\text{PO}_4)_6$ solid ($146.0 \text{ kJ}\cdot\text{mol}^{-1}$). These results are due to the effective reduction of electrostatic interaction of Ca^{2+} . While the $\text{CaZr}_4(\text{PO}_4)_6$ solid contains two kinds of high valent cation (Zr^{4+} and P^{5+}), the $(\text{Ca}_{0.05}\text{Hf}_{0.95})_{4/3.9}\text{Nb}(\text{PO}_4)_3$ solid is composed of three kinds of high valent cation (Nb^{5+} in addition to Hf^{4+} , P^{5+}). The presence of high valent Nb^{5+} cation in the lattice which effectively reduced the electrostatic interaction, allowing smooth migration of the Ca^{2+} cation in the solid. Furthermore, despite the ionic radius of Ca^{2+} (0.114 nm [coordination number = 6] [43]) is larger than Mg^{2+} (0.086 nm [coordination number = 6] [43]), the ionic conductivity and activation energy of $(\text{Ca}_{0.05}\text{Hf}_{0.95})_{4/3.9}\text{Nb}(\text{PO}_4)_3$ ($5.21 \times 10^{-5} \text{ S}\cdot\text{cm}^{-1}$, $55.80 \text{ kJ}\cdot\text{mol}^{-1}$) and $(\text{Mg}_{0.05}\text{Hf}_{0.95})_{4/3.9}\text{Nb}(\text{PO}_4)_3$ ($6.04 \times 10^{-5} \text{ S}\cdot\text{cm}^{-1}$, $55.76 \text{ kJ}\cdot\text{mol}^{-1}$) solids exhibited similar values. Since the electronegativity of calcium ion (Ca^{2+} , 1.00) is smaller than that of magnesium ion (Mg^{2+} , 1.31), electrostatic interaction of $\text{Ca}^{2+}-\text{O}^{2-}$ bonding is weaker than $\text{Mg}^{2+}-\text{O}^{2-}$ bonding in the structures. In other words, the weak electrostatic interaction of the $\text{Ca}^{2+}-\text{O}^{2-}$ bonding has made it easier for Ca^{2+} ion to migrate in the $(\text{Ca}_{0.05}\text{Hf}_{0.95})_{4/3.9}\text{Nb}(\text{PO}_4)_3$ solid.

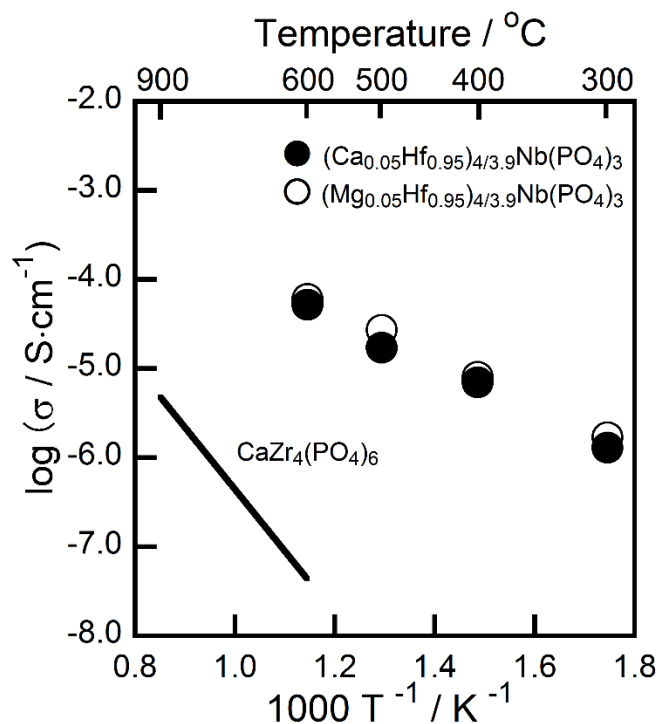


Figure 2.5. Temperature dependencies of the ion conductivity for the $(M_{0.05}Hf_{0.95})_{4/3.9}Nb(PO_4)_3$ ($M = Ca, Mg$) and $CaZr_4(PO_4)_6$ solids.

2.4 Conclusions

A new NASICON-type divalent Ca^{2+} cation conductor, $(Ca_{0.05}Hf_{0.95})_{4/3.9}Nb(PO_4)_3$, was successfully synthesized by introducing Ca^{2+} , which has the lower electronegativity than Mg^{2+} , into the Hf^{4+} ion sites of the $HfNb(PO_4)_3$ solid. Although ionic radius of Ca^{2+} cation is larger than Mg^{2+} cation, the $(Ca_{0.05}Hf_{0.95})_{4/3.9}Nb(PO_4)_3$ solid ion conductivity and activation energy exhibited similar results with the $(Mg_{0.05}Hf_{0.95})_{4/3.9}Nb(PO_4)_3$ solid, due to the weaker electrostatic interaction than that of $Mg^{2+}-O^{2-}$ bonding.

Chapter 3

Effect of the Conducting Divalent Ion Species on the Ion Conducting in Solid Electrolytes with NASICON-type Structure

3.1 Introduction

In order to clarify the effect of migrating divalent cation species on the ion conducting properties, it is necessary to compare the conducting characteristics of various divalent cation conductors. The divalent cation conductors described in Chapters 1 and 2 and previous reports, are obtained by the partial substitution of the Hf^{4+} ion sites in the $\text{HfNb}(\text{PO}_4)_3$ solid with the lower-valence M^{2+} ($\text{M} = \text{Ni}, \text{Mg}$ [9], Ca) ion with the strategy of changing the conducting ion species from the high-valence Hf^{4+} ion to the lower-valence M^{2+} ion.

In this chapter, I prepared the Sr^{2+} and Ba^{2+} ion conductors with the NASICON-type structure in addition to Ni^{2+} , Mg^{2+} and Ca^{2+} ion conductors for investigating the relationship between the M^{2+} cation conductivity and the ionic size of migrating divalent cation species for the $(\text{M}_{0.05}\text{Hf}_{0.95})_{4/3.9}\text{Nb}(\text{PO}_4)_3$ ($\text{M} = \text{Ni}, \text{Mg}, \text{Ca}, \text{Sr}, \text{Ba}$) solids.

3.2 Experimental Procedure

$(\text{M}_x\text{Hf}_{1-x})_{4/(4-2x)}\text{Nb}(\text{PO}_4)_3$ ($\text{M} = \text{Sr}, \text{Ba}$) solids were synthesized by the conventional wet coprecipitation method using $\text{Sr}(\text{NO}_3)_2$, $\text{Ba}(\text{NO}_3)_2$, HfCl_4 , NbCl_5 , and $(\text{NH}_4)_2\text{HPO}_4$. $(\text{NH}_4)_2\text{HPO}_4$ was added into an ethanol solution containing stoichiometric amount of $\text{M}(\text{NO}_3)_2$ ($\text{M} = \text{Sr}, \text{Ba}$), HfCl_4 ,

and NbCl_5 . After stirring and drying at 130 °C, the obtained powder was pre-calcined at 600 °C for 6 h, and then calcined at 1100–1350 °C for 6 h in the air atmosphere.

Crystal structure of the calcined samples was identified by X-ray powder diffraction (XRD; SmartLab, Rigaku) measurement using $\text{Cu-K}\alpha$ radiation (40 kV, 40 mA). The lattice volume of the calcined samples was calculated from the XRD peak angles, which were refined using $\alpha\text{-Al}_2\text{O}_3$ as an internal standard. After identifying the crystal phase of the sample powders, the powders were pelletized and sintered at 1200–1350 °C for 12 h in air atmosphere.

The ac conductivity (σ_{ac}) of the sintered pellet was measured by complex impedance method (1260 Impedance/Gain-Phase Analyzer, Solartron) at temperatures between 300 °C and 600 °C in the air atmosphere. In order to identify the conducting species for the sample pellets, ac and dc conductivities were measured at 600 °C in various oxygen partial pressure conditions from 10^{-17} to 10^5 Pa, which were regulated by O_2 , Ar, CO-CO_2 mixture gas, and air. The cation transference number was calculated from the equation of $\{1 - (\sigma_{\text{dc}}/\sigma_{\text{ac}})\}$.

The dc electrolysis of sintered pellets was carried out by applying dc voltage higher than the decomposition voltage, and then the elemental distribution in the electrolyzed sample pellets was observed by cross-sectional line analysis using energy dispersive X-ray spectroscopy (EDX; SSX-550, Shimadzu).

3.3 Results and Discussion

3.3.1. $(\text{Sr}_x\text{Hf}_{1-x})_{4/(4-2x)}\text{Nb}(\text{PO}_4)_3$ ($0.01 \leq x \leq 0.10$) solids

From the XRD measurement of the $(\text{Sr}_x\text{Hf}_{1-x})_{4/(4-2x)}\text{Nb}(\text{PO}_4)_3$ ($0.01 \leq x \leq 0.10$) solids, the single-phase of NASICON-type structure was obtained for the samples with $x \leq 0.05$ (Figure 3.1). Figure 3.2 shows the compositional dependencies of the lattice volume and the ac conductivity of the $(\text{Sr}_x\text{Hf}_{1-x})_{4/(4-2x)}\text{Nb}(\text{PO}_4)_3$ ($0.01 \leq x \leq 0.10$) solids calcined at 1200 °C. The lattice volume of the single-phase samples increased up to $x = 0.05$, because Sr^{2+} (0.132 nm, [CN=6] [43]) is larger than that of Hf^{4+} cation (0.085 nm, [CN=6] [43]). This result indicates that the solid solubility limit composition of the $(\text{Sr}_x\text{Hf}_{1-x})_{4/(4-2x)}\text{Nb}(\text{PO}_4)_3$ solids is $x = 0.05$. In addition, the Sr^{2+} cation conductivity was increased with the Sr^{2+} cation content up to the solubility limit compositions.

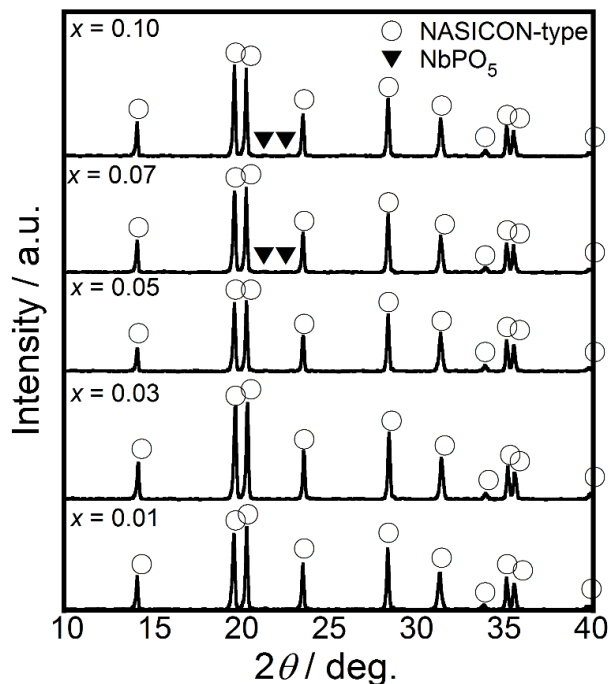


Figure 3.1. XRD patterns of $(\text{Sr}_x\text{Hf}_{1-x})_{4/(4-2x)}\text{Nb}(\text{PO}_4)_3$ solids.

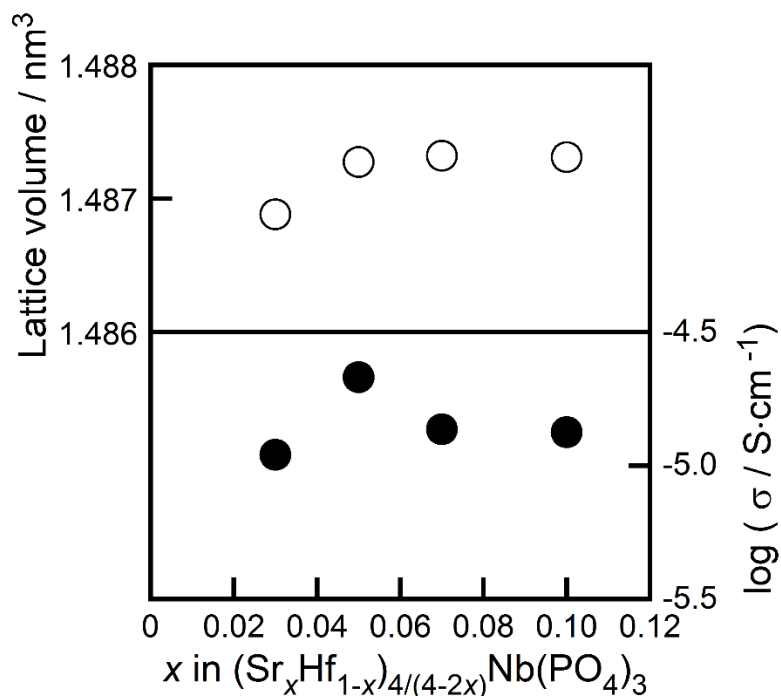


Figure 3.2. Compositional dependencies of the lattice volume (○) and the ac conductivity at 600 °C (●) of the $(\text{Sr}_x\text{Hf}_{1-x})_{4/(4-2x)}\text{Nb}(\text{PO}_4)_3$ solids.

Figure 3.3 depicts the result of EDX line analysis for the electrolyzed pellet after applying a dc voltage of 5 V for 7 days at 600 °C. Only Sr was clearly segregated at the cathodic surface of the sample pellet, which indicates that only Sr^{2+} ions migrated inside the $(\text{Sr}_{0.05}\text{Hf}_{0.95})_{4/3.9}\text{Nb}(\text{PO}_4)_3$ solid. Furthermore, the cation transference number estimated from the $\sigma_{\text{dc}} / \sigma_{\text{ac}}$ conductivity ratio was higher than 0.99. From these results, it was demonstrated that the $(\text{Sr}_{0.05}\text{Hf}_{0.95})_{4/3.9}\text{Nb}(\text{PO}_4)_3$ solid is a Sr^{2+} cation conductor.

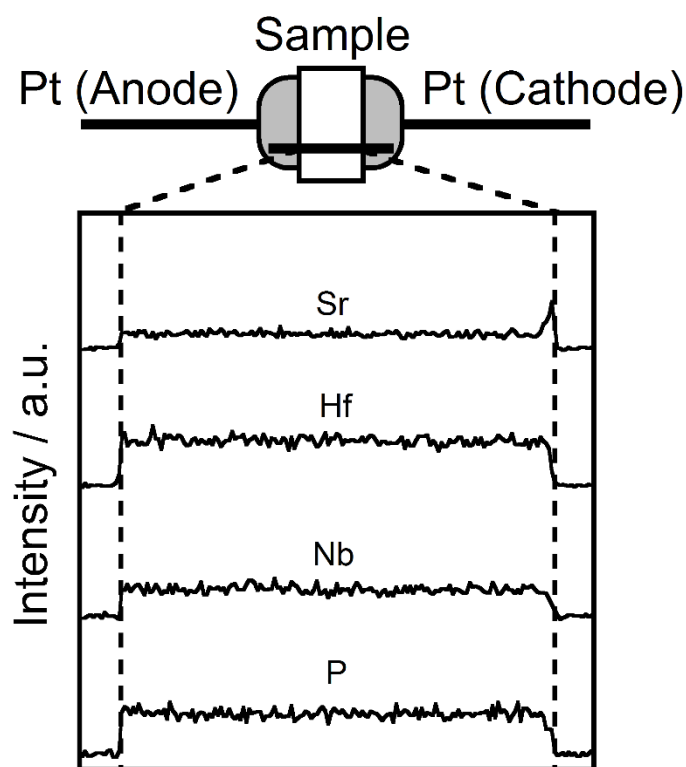


Figure 3.3. Results of EDX line analysis for the electrolyzed $(\text{Sr}_{0.05}\text{Hf}_{0.95})_{4/3.9}\text{Nb}(\text{PO}_4)_3$ solid.

3.3.2. $(\text{Ba}_x\text{Hf}_{1-x})_{4/(4-2x)}\text{Nb}(\text{PO}_4)_3$ ($0.01 \leq x \leq 0.05$) solids

Figure 3.4 shows XRD patterns of the $(\text{Ba}_x\text{Hf}_{1-x})_{4/(4-2x)}\text{Nb}(\text{PO}_4)_3$ ($0.01 \leq x \leq 0.05$) solids. In the case for the $(\text{Ba}_x\text{Hf}_{1-x})_{4/(4-2x)}\text{Nb}(\text{PO}_4)_3$ samples, the single-phase NASICON-type solids were not obtained for all composition studied due to too large ionic radius (0.149 nm, [43]) of Ba^{2+} .

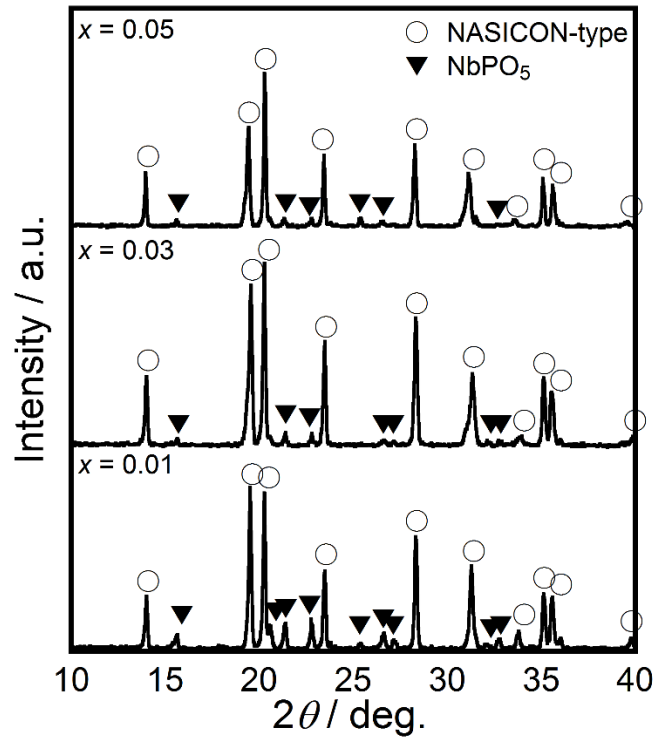


Figure 3.4. XRD patterns of $(\text{Ba}_x\text{Hf}_{1-x})_{4/(4-2x)}\text{Nb}(\text{PO}_4)_3$ solids.

3.3.3. Comparison of $(\text{M}_x\text{Hf}_{1-x})_{4/(4-2x)}\text{Nb}(\text{PO}_4)_3$ solids (M = Ni, Mg, Ca, Sr)

Figure 3.5 depicts the temperature dependence of divalent cation conductivity for the $(\text{Ni}_{0.06}\text{Hf}_{0.94})_{4/3.88}\text{Nb}(\text{PO}_4)_3$, $(\text{Mg}_{0.1}\text{Hf}_{0.9})_{4/3.8}\text{Nb}(\text{PO}_4)_3$, $(\text{Ca}_{0.05}\text{Hf}_{0.95})_{4/3.9}\text{Nb}(\text{PO}_4)_3$, and $(\text{Sr}_{0.05}\text{Hf}_{0.95})_{4/3.9}\text{Nb}(\text{PO}_4)_3$ solids which are the solids with the solid solubility composition with the corresponding data for the $\text{MZr}_4(\text{PO}_4)_6$ (M = Ni, Mg, Ca, Sr) solids. The divalent M^{2+} ion conductivities of the $(\text{Ni}_{0.06}\text{Hf}_{0.94})_{4/3.88}\text{Nb}(\text{PO}_4)_3$, $(\text{Mg}_{0.1}\text{Hf}_{0.9})_{4/3.8}\text{Nb}(\text{PO}_4)_3$, $(\text{Ca}_{0.05}\text{Hf}_{0.95})_{4/3.9}\text{Nb}(\text{PO}_4)_3$, and $(\text{Sr}_{0.05}\text{Hf}_{0.95})_{4/3.9}\text{Nb}(\text{PO}_4)_3$ solids are extraordinarily higher than those of the $\text{MZr}_4(\text{PO}_4)_6$ (M = Ni, Mg, Ca, Sr) solids at 600 °C. This is due to synthesized samples having the well-ordered three-dimensional NASICON-type structure with small structural distortion. In addition, the existence of various kinds of high valence cations (Hf^{4+} , Nb^{5+} , P^{5+}) in the structure effectively reduced the electrostatic interaction between the migrating M^{2+} cations and surrounding O^{2-} anions.

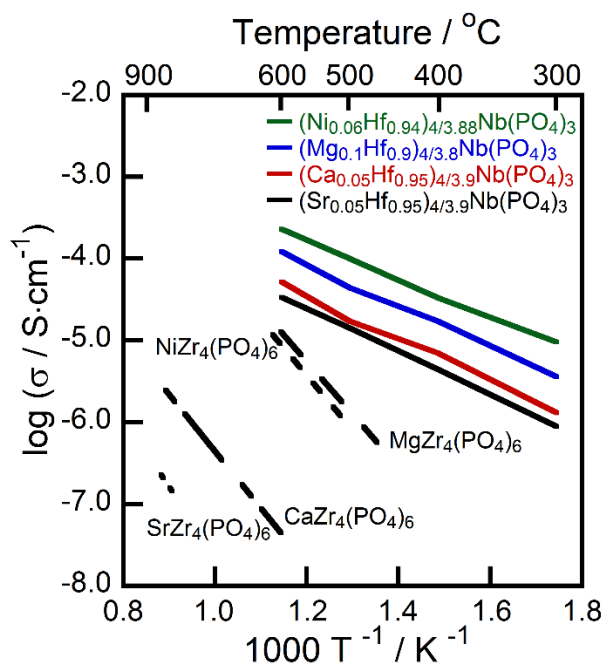


Figure 3.5. Temperature dependence of the ac conductivity for the $(\text{Ni}_{0.06}\text{Hf}_{0.94})_{4/3.88}\text{Nb}(\text{PO}_4)_3$, $(\text{Mg}_{0.1}\text{Hf}_{0.9})_{4/3.8}\text{Nb}(\text{PO}_4)_3$, $(\text{Ca}_{0.05}\text{Hf}_{0.95})_{4/3.9}\text{Nb}(\text{PO}_4)_3$, $(\text{Sr}_{0.05}\text{Hf}_{0.95})_{4/3.9}\text{Nb}(\text{PO}_4)_3$, and $\text{MZr}_4(\text{PO}_4)_6$ ($\text{M} = \text{Ni, Mg, Ca, Sr}$) solids.

The ion conduction in solids is also influenced by the crystallinity of the sample, which is an important factor especially for such well-ordered three-dimensional network structure. The distortion of the crystal structure causes the deterioration of conducting pathway and consequently makes it difficult for ion to migrate. Since the crystallinity of the sample is strongly dependent on the sintering temperature, I have to satisfy the sintering condition for discussing the relationship between the cation conduction and the ionic size of conducting cation species. The described M^{2+} cation conductivities of the $(\text{Ni}_{0.06}\text{Hf}_{0.94})_{4/3.88}\text{Nb}(\text{PO}_4)_3$, $(\text{Mg}_{0.1}\text{Hf}_{0.9})_{4/3.8}\text{Nb}(\text{PO}_4)_3$, $(\text{Ca}_{0.05}\text{Hf}_{0.95})_{4/3.9}\text{Nb}(\text{PO}_4)_3$, and $(\text{Sr}_{0.05}\text{Hf}_{0.95})_{4/3.9}\text{Nb}(\text{PO}_4)_3$ solids were the samples with solid solubility composition and sintered at optimum temperature; i.e. 1300 °C for Ni and Mg, 1200 °C for Ca and Sr. In the case for the Ca

and Sr samples, when the calcination temperature rises higher than 1200 °C, the impurity phase of NbPO₅ appeared in addition to the NASICON-type solid due to the sample decomposition. Therefore, since it is essential to compare the conductivity of the solids with the same M²⁺ cation concentration and sintering temperature for discussing the effect of ionic size of conducting M²⁺ on the conducting properties in NASICON-type solids, I compared the conducting properties of the (M_{0.05}Hf_{0.95})_{4/3.9}Nb(PO₄)₃ (M = Ni, Mg, Ca, Sr) solids, whose composition was within the solid solubility one for all systems, sintered at 1200 °C. Furthermore, I introduced a concept of the relative volume ratio of the divalent cation to lattice ($A \text{ ratio} = V_{\text{ion}} / V_{\text{lattice}}$) [41, 48, 49] which should refer to the relative size of conducting ion species to the conducting pathway.

Figure 3.6 depicts the M²⁺ ionic radius dependencies of the *A* ratio, ion conductivity at 600 °C, and activation energy for M²⁺ migration. The *A* ratio is linearly increased with increase of M²⁺ ionic radius, meaning that there is no proportional relation between the expansion degrees of lattice volume and conducting ion volume. In other words, the sample with smaller divalent M²⁺ cation has relatively large conducting pathway in its structure. Since the large conducting pathway is effective for smooth ion migration, a monotonous decrease in conductivity was observed with increasing the ionic radius of M²⁺ ion, which is opposite tendency of *A* ratio change. The M²⁺ conductivity at 600 °C and the activation energy of the (M_{0.05}Hf_{0.95})_{4/3.9}Nb(PO₄)₃ (M = Ni, Mg, Ca, Sr) solids are listed in Table 3.1. Although the difference in activation energy for the samples with M = Mg and Ca was small, a clear order was recognized. If the ion conduction of the crystal lattice is influenced only by the relationship between ionic size and lattice volume (*A* ratio) of the conducting species, ion conductivity and activation energy for the sample with Ca²⁺ are expected to be more low and high, respectively. As mentioned in the Chapter 2, higher Ca²⁺ conducting property compared was caused by a weak electrostatic interaction between Ca²⁺ and surrounding O²⁻ ions in the structure. Generally, ionic-bonding is weaker than covalent-bonding in solid materials. Since the electronegativity of calcium ion (Ca²⁺, 1.00) is smaller than that of magnesium ion (Mg²⁺, 1.31), covalency of Ca–O bonding is

small compared to Mg–O bonding. In other words, the interaction of Ca–O bonding is weaker than Mg–O bonding in solid. Therefore, Ca^{2+} ions can smoothly migrate in the $(\text{Ca}_{0.05}\text{Hf}_{0.95})_{4/3.9}\text{Nb}(\text{PO}_4)_3$ solid.

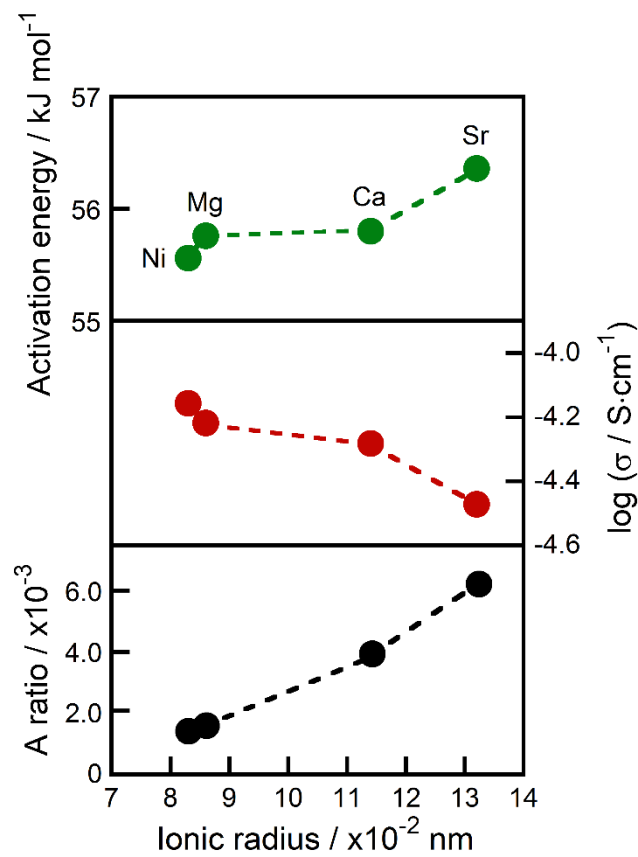


Figure 3.9. The ionic radius of M^{2+} dependencies of the A ratio, the ion conductivity and the activation energy.

Table 3.1. Conductivity and activation energy of the $(M_{0.05}Hf_{0.95})_{4/3.9}Nb(PO_4)_3$ ($M = Ni, Mg, Ca, Sr$) solids

Sample	Conductivity S / cm	Activation energy kJ / mol
$(Ni_{0.05}Hf_{0.95})_{4/3.9}Nb(PO_4)_3$	6.96×10^{-5}	55.56
$(Mg_{0.05}Hf_{0.95})_{4/3.9}Nb(PO_4)_3$	6.04×10^{-5}	55.76
$(Ca_{0.05}Hf_{0.95})_{4/3.9}Nb(PO_4)_3$	5.21×10^{-5}	55.80
$(Sr_{0.05}Hf_{0.95})_{4/3.9}Nb(PO_4)_3$	3.37×10^{-5}	56.36

3.4 Conclusions

I have additionally synthesized the divalent M^{2+} cation conducting solid electrolytes of the $(Sr_xHf_{1-x})_{4/(4-2x)}Nb(PO_4)_3$ solids with NASICON-type structures for discussing the divalent cation conduction in NASICON-type $(M_xHf_{1-x})_{4/(4-2x)}Nb(PO_4)_3$ ($M = Ni, Mg, Ca, Sr$) solids.

From the investigation of the ion conducting properties in the NASICON-type $(M_{0.05}Hf_{0.95})_{4/3.9}Nb(PO_4)_3$ ($M = Ni, Mg, Ca, Sr$) solids, it was found that the conducting property is mainly influenced by the relative size of the conduction pathway, and also by the electronegativity of conducting species from the comparison of the $(Mg_{0.05}Hf_{0.95})_{4/3.9}Nb(PO_4)_3$ and $(Ca_{0.05}Hf_{0.95})_{4/3.9}Nb(PO_4)_3$ solids.

Summary

In the study of this thesis, new divalent cation conductors with high conductivity were developed, and the key factors which determine the divalent cation conduction were clarified. For this purpose, various kinds of NASICON-type divalent cation conductors were synthesized and their conducting properties were discussed from the view point of constituent cations.

The results and conclusions obtained through this work are summarized as follows:

Chapter 1

For achieving high conductivity at moderate temperatures, Ni^{2+} cations having a smaller ionic radius than that of Mg^{2+} cations were introduced into the Hf^{4+} ion sites of the $\text{HfNb}(\text{PO}_4)_3$ solid. The introduction of Ni^{2+} cation into the $\text{HfNb}(\text{PO}_4)_3$ solid effectively reduced the activation energy and enhanced the ion conductivity due to the small ionic radius of Ni^{2+} and the existence of high-valence cations. The $(\text{Ni}_{0.06}\text{Hf}_{0.94})_{4/3.88}\text{Nb}(\text{PO}_4)_3$ solid showed the lowest activation energy and the highest Ni^{2+} cation conductivity at 600°C .

Chapter 2

A new divalent Ca^{2+} ion conductor with high ion conductivity, NASICON-type $(\text{Ca}_{0.05}\text{Hf}_{0.95})_{4/3.9}\text{Nb}(\text{PO}_4)_3$ solid, was successfully developed. The ion conductivity of the $(\text{Ca}_{0.05}\text{Hf}_{0.95})_{4/3.9}\text{Nb}(\text{PO}_4)_3$ solid was about 1000 times higher than that of the $\text{CaZr}_4(\text{PO}_4)_6$ solid previously reported. From the results obtained in this study, it was found that high ion conduction can be obtained by the selection of divalent cation with small electronegativity as the conducting species.

Chapter 3

For discussing the effect of the ionic size of the conducting divalent cation species on the ion conduction in NASICON-type structure, I compared the conducting properties of the $(M_{0.05}Hf_{0.95})_{4/3.9}Nb(PO_4)_3$ ($M = Ni, Mg, Ca, Sr$) solids, which possess the same constituent ions except for the conducting cation species. As a result, it was clear that the conducting properties were mainly influenced by the relative size of the conduction pathway in the NASICON-type structure. In addition, the electronegativity of conducting species also affected the divalent cation conductivity.

References

- [1] K. Takada, *Acta Mater.*, **61**, 759, (2013).
- [2] M. Tatsumisago, M. Nagao, A. Hayashi, *J. Asian Ceram. Soc.*, **1**, 17 (2013).
- [3] S. Teng, J. Tan, A. Tiwari, *Curr. Opin. Solid State Mater. Sci.*, **18**, 29 (2014).
- [4] X. Xu, T. Yang, M. Shui, Z. Lu, S. Gao, J. Shu, W. Zheng, L. Cheng, L. Feng, Y. Ren, *Ceram. Int.*, **40**, 3819 (2014).
- [5] S. Tamura, Y. Okada, N. Imanaka, *Electrochemistry*, **82**, 830 (2014).
- [6] M.L. Aubrey, R. Ameloot, B.M. Wiers, J.R. Long, *Energy Environ. Sci.*, **7**, 667 (2014).
- [7] Y. Shao, N.N. Rajput, J. Hu, M. Hu, T. Liu, Z. Wei, M. Gu, X. Deng, S. Xu, K.S. Han, J. Wang, Z. Nie, G. Li, K.R. Zavadil, J. Xiao, C. Wang, W.A. Henderson, J.G. Zhang, Y. Wang, K.T. Mueller, K. Persson, J. Liu, *Nano Energy*, **12**, 750 (2015).
- [8] Z. Zhao-Karger, X. Zhao, D. Wang, T. Diemant, R.J. Behm, M. Fichtner, *Adv Energy Mater.*, **5**, 1401155 (2015).
- [9] S. Tamura, M. Yamane, Y. Hoshino, N. Imanaka, *J. Solid State Chem.*, **235**, 7 (2016).
- [10] G.C. Farrington, B. Dunn, *Solid State Ionics*, **7**, 274 (1982).
- [11] D.W. Stricker, W.G. Carlson, *J. Am. Ceram. Soc.*, **47**, 122 (1964).
- [12] B. Dunn, R.M. Ostrom, R. Seevers, G.C. Farrington, *Solid State Ionics*, **5**, 203 (1981).
- [13] S. Ikeda, M. Takahashi, J. Ishikawa, K. Ito, *Solid State Ionics*, **23**, 125 (1987).
- [14] K. Nomura, S. Ikeda, K. Ito, *Bull. Chem. Soc. Jpn.*, **65**, 3221 (1992).
- [15] K. Nomura, S. Ikeda, K. Ito, H. Einaga, *Solid State Ionics*, **61**, 293 (1993).
- [16] S. Ikeda, S. Kato, K. Nomura, K. Ito, H. Einaga, *Solid State Ionics*, **70-71**, 569 (1994).
- [17] N. Imanaka, S. Tamura, *Bull. Chem. Soc. Jpn.*, **84**, 357 (2011).
- [18] N. Nunotani, S. Tamura, N. Imanaka, *Electrochemistry*, **80**, 743 (2012).

- [19] N. Nunotani, T. Ohsaka, S. Tamura, N. Imanaka, *ECS Electrochem. Lett.*, **1**, A66 (2012).
- [20] N. Nunotani, M. Sawada, S. Tamura, N. Imanaka, *Bull. Chem. Soc. Jpn.*, **83**, 415 (2010).
- [21] N. Nunotani, S. Tamura, N. Imanaka, *Chem. Lett.*, **38**, 658 (2009).
- [22] S. Tamura, T. Itano, N. Nunotani, N. Imanaka, *Electrochem. Solid State Lett.*, **12**, F5 (2009).
- [23] N. Nunotani, S. Tamura, N. Imanaka, *Chem. Mater.*, **21**, 579 (2009).
- [24] Y. Hasegawa, S. Tamura, M. Sato, N. Imanaka, *Bull. Chem. Soc. Jpn.*, **81**, 521 (2008).
- [25] S. Tamura, S. Yamamoto, N. Imanaka, *J. New Mat. Electrochem. Syst.*, **11**, 1 (2008).
- [26] Y. Hasagawa, T. Hoshiyama, S. Tamura, N. Imanaka, *J. New Mat. Electrochem. Syst.*, **10**, 177 (2007).
- [27] N. Imanaka, S. Tamura, T. Itano, *J. Am. Chem. Soc.*, **129**, 5338 (2007).
- [28] Y. Hasegawa, N. Imanaka, *J. Alloy. Compd.*, **408-412**, 661 (2006).
- [29] Y. Hasegawa, S. Tamura, N. Imanaka, *J. New Mat. Electrochem. Syst.*, **8**, 203 (2005).
- [30] Y. Hasegawa, N. Imanaka, *Solid State Ionics*, **176**, 2499 (2005).
- [31] N. Imanaka, *J. Ceram. Soc. Jpn.*, **113**, 387 (2005).
- [32] Y. Hasegawa, S. Tamura, N. Imanaka, G. Adachi, *J. Alloys Compd.*, **379**, 262 (2004).
- [33] Y. Hasegawa, S. Tamura, N. Imanaka, G. Adachi, Y. Takano, T. Tsubaki, K. Sekizawa, *J. Alloys Compd.*, **375**, 212 (2004).
- [34] Y. Hasegawa, N. Imanaka, G. Adachi, *J. Solid State Chem.*, **171**, 387 (2003).
- [35] N. Imanaka, T. Ueda, G. Adachi, *J. Solid State Electrochem.*, **7**, 239 (2003).
- [36] N. Imanaka, Y. Hasegawa, M. Yamaguchi, M. Itaya, S. Tamura, G. Adachi, *Chem. Mater.*, **14**, 4481 (2002).
- [37] M. Itaya, N. Imanaka, G. Adachi, *Solid State Ionics*, **154-155**, 319 (2002).
- [38] S. Tamura, N. Imanaka, G. Adachi, *Solid State Ionics*, **154-155**, 767 (2002).
- [39] N. Imanaka, M. Itaya, G. Adachi, *Mater. Lett.*, **57**, 209 (2002).
- [40] G. Adachi, N. Imanaka, S. Tamura, *Chem. Rev.*, **102**, 2426 (2002).

- [41] N. Imanaka, G. Adachi, *J. Alloys Compd.*, **344**, 137 (2002).
- [42] N. Imanaka, M. Itaya, G. Adachi, *Mater. Lett.*, **53**, 1 (2002).
- [43] R.D. Shannon, *Acta Crystallogr. Sect.*, **A32**, 751 (1976).
- [44] J.C. Jesus, I. Gonzalez, A. Quevedo, T. Puerta, *J. Mol. Catal. A: Chem.*, **228**, 288 (2005).
- [45] L.J. Matienzo, L.I. Yin, S.O. Grim, W.E. Swartz, *Inorg. Chem.*, **12**, 2766 (1973).
- [46] V. Biju, M.A. Khadar, *J. Nanopart. Res.*, **4**, 248 (2002).
- [47] Y. Kobayashi, T. Egawa, S. Tamura, N. Imanaka, G. Adachi, *Chem. Mater.*, **9**, 1652 (1997).
- [48] H. Aono, N. Imanaka, G. Adachi, *Accounts Chem. Res.*, **27**, 265 (1994).
- [49] S. Tamura, N. Imanaka, G. Adachi, *J. Alloys Compd.*, **323-324**, 540 (2001).

Acknowledgements

The author would like to express his heartfelt gratitude to Professor Dr. Nobuhito Imanaka, Department of Applied Chemistry, Graduate School of Engineering, Osaka University, for his continuous guidance, many invaluable suggestions, and science encouragement throughout the work.

The author is very grateful to Dr. Shinji Tamura, Department of Applied Chemistry, Graduate School of Engineering, Osaka University, for his continuous guidance and stimulating discussions for carrying out this work. The author is also indebted to Dr. Naoyoshi Nunotani, Department of Applied Chemistry, Graduate School of Engineering, Osaka University, for his helpful suggestions and apposite advice.

The author is deeply grateful to Professor Dr. Susumu Kuwabata, and Professor Dr. Ken-ichi Machida, Department of Applied Chemistry, Graduate School of Engineering, Osaka University, for reviewing this thesis and giving their valuable comments.

Special thanks should be given to author's co-workers, Ms. Megumi Yamane, Mr. Yusuke Kikkawa, Mr. Muhammad Radzi Iqbal, Mr. Masanori Umeda, Mr. Shota Yamauchi, Mr. Takuya Morioki, Mr. Shohei Saeki, Mr. Kentaro Yamada, Mr. Koki Yoshikawa, and Mr. Kenji Matsuo for their helpful assistance and support in the course of this work, and the other members of the research group under direction of Professor Dr. Nobuhito Imanaka, Osaka University.

Finally, the author would like to extend deep gratitude to his parents, Mr. Janghyun Lee and Mrs. Eunju Park, his sister, Mrs. Jiyeong Lee, and all members of his family for their encouragement, continuous understanding, and perpetual supports.